Impact of the valley degree of freedom on the control of donor electrons near a Si/SiO_2 interface

A. Baena,[1] A. L. Saraiva,[2] Belita Koiller,[2] and M.J. Calderón[1]

[1]*Instituto de Ciencia de Materiales de Madrid, ICMM-CSIC, Cantoblanco, E-28049 Madrid, Spain*
[2]*Instituto de Fisica, Universidade Federal do Rio de Janeiro, Caixa Postal 68528, 21941-972 Rio de Janeiro, Brazil*

(Dated: March 1, 2013)

We analyze the valley composition of one electron bound to a shallow donor close to a Si/barrier interface as a function of an applied electric field. A full six-valley effective mass model Hamiltonian is adopted. For low fields, the electron ground state is essentially confined at the donor. At high fields the ground state is such that the electron is drawn to the interface, leaving the donor practically ionized. Valley splitting at the interface occurs due to the valley-orbit coupling, $V_{\rm vo}^I = |V_{\rm vo}^I|e^{i\theta}$. At intermediate electric fields, close to a characteristic shuttling field, the electron states may constitute hybridized states with valley compositions different from the donor and the interface ground states. The full spectrum of energy levels shows crossings and anti-crossings as the field varies. The degree of level repulsion, thus the width of the anti-crossing gap, depends on the relative valley compositions, which vary with $|V_{\rm vo}^I|$, θ and the interface-donor distance. We focus on the valley configurations of the states involved in the donor-interface tunneling process, given by the anti-crossing of the three lowest eigenstates. A sequence of two anti-crossings takes place and the complex phase θ affects the symmetries of the eigenstates and level anti-crossing gaps. We discuss the implications of our results on the practical manipulation of donor electrons in Si nanostructures.

PACS numbers: 85.30.-z, 85.35.Gv, 03.67.Lx

I. INTRODUCTION

The search for a functional quantum computer (QC) started in the mid-nineties, and by the year 2000 many systems had been considered as candidates for its physical implementation.[1] Among them, the 1998 proposal for a Si-based QC by Kane[2] raised special interest due to objective and relevant factors favoring Si, such as the accumulated know-how in processing Si for advanced device applications, the relatively long spin coherence times and the possibility of isotopic purification processing, further increasing coherence times.[3]

On the other hand, the conduction electrons in Si are not in a well defined single Bloch state. Instead, the Si conduction band is six-fold degenerate, with minima (valleys) along the x, y and z crystallographic directions. This imposes limitations to the spin manipulation and coherence.[4]

It was recently proposed to encode quantum information directly into the valley degree of freedom, converting the spurious valley Hilbert subspace into a useful ingredient for a QC.[5] Naturally, this raises fundamental questions, such as how to promote controlled inter-valley transitions, to what extent valley degeneracy can be lifted, and how sensitive such operations are to fabrication-related parameters. The valley degree of freedom also affects transport properties in Si nanostructures: valley degeneracy has been recently shown to produce a valley Kondo effect in a singly doped Si fin field effect transistor.[6]

We study here the valley degree of freedom for one electron bound to a donor — more specifically substitutional P in Si — tunnel-coupled to a (001) Si/SiO_2 interface at a distance d from the donor. The barrier material is taken to be SiO_2 for definiteness, but it could in principle be any high quality interface, such as Si/SiGe. The evolution of the inequivalent valley contributions is obtained by mapping the low-lying manifold (following in more detail the three lowest energy states) as an electric field pulls the electron away from its "hydrogenic" configuration at the donor site towards the state at the interface.

A ground state electron confined in the direction perpendicular to the interface in the triangular potential formed by the barrier and the electric field [see Fig. 1(a)], still remains bound to the donor core potential, leading to localization in the in-plane direction.[7,8] For low fields, the electron in the ground state is essentially confined at the donor, where the lowest energy manifold is split by the tetrahedral crystal field environment into states with distinct contributions from the six valleys. In particular, the ground state at the donor is a non-degenerate symmetric combination of the six valleys.

At high enough fields, the donor is ionized, and its electron is shuttled to the interface. At the interface, the valley levels split into a four-fold degenerate excited state, consisting of $\pm x$ and $\pm y$ Bloch states, and a lower manifold spanned by the $\pm z$ valleys. The two lowest levels are only slightly separated due to the abrupt interface breaking the z reflection symmetry (generally less than 1 meV separation[9–14]).

These relatively simple and well understood valley compositions at interfaces and isolated donors could lead to a variety of compositions at intermediate fields, as illustrated by the main panel in Fig. 1. The lines are symmetry-allowed paths connecting energy levels from

the low-field (right of the panel) to the high-field (left) regime: one may anticipate a rich variety of behaviors and formation of hybrid donor-interface states. Each level crossing or anti-crossing as the field varies may change the valley compositions of the involved states.

The Stark shifted spectrum of P donors in bulk Si (no barrier material) is discussed in Ref. [15]. The effective mass approach is adopted and the envelope functions are expressed as a combination of atomic-like orbitals. The same group considered later the Stark effect for P donors at the center of Si nanospheres embedded in a barrier material.[16] The quasi-spherical symmetry of the problem without field allows the assignement of hydrogenic quantum numbers to the interface states. Tight-binding calculations for systems more directly related to the present geometry were reported in Ref. [17]. In these references elaborate numerical procedures are adopted leading to accurate results. Here we get good qualitative agreement for the spectrum in comparison with these previous works, and we explore a complementary aspect - namely the valley-composition evolution of the low-lying states under an increasing external field. The same geometry has been previously studied in a two-valley model $\{(000001), (000010)\}$ where the valley-composition analysis is not accessible.[18]

We discuss here the evolution of the valley quantum number as a function of the electric field for field values in the range where the hybridization between donor and interface states takes place. We show that the phase of the interface valley-orbit coupling plays an important role in defining the gap amplitudes, affecting manipulation capabilities for the donor electrons. Our model sheds light to the qualitative features of the level diagrams shown in Refs. [15,17], and permits to predict the expected diagrams for various geometries of the donor/barrier problem. Our aim is to get a clear description of the changes in symmetry and valley composition of the states involved in the donor-interface electron shuttling problem. Our results may be useful for donor electron valley manipulation via an applied field.

This paper is organized as follows. In Sec. II the system is described and a 6-valley effective mass model-Hamiltonian for the donor electron under an applied electric field is explained. In Sec. III, our results for the electric field dependence of the low-lying spectrum and of the valley composition of the three lowest electronic eigenstates are presented. We conclude in Sec. IV with a discussion of the implications of these results on the practical manipulation of donor electrons in Si nanostructures.

II. MODEL

We consider a single electron bound to a substitutional P donor at $z = 0$ near a Si (001) / SiO_2 interface at $z = -d$ and under an applied uniform electric field perpendicular to the interface, $\vec{F} = F\hat{z}$ pointing from the

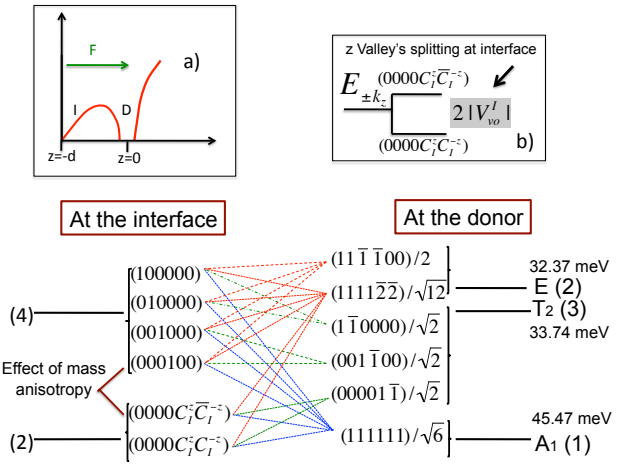

FIG. 1: (Color online) (a) Double well potential in the z-direction formed by the Coulombic donor potential plus the triangular interface/electric field potential. d is the distance between the donor and interface. (Main panel) Symmetry of levels at the donor and at the interface. Every level is described by six coefficients corresponding to the six valleys of Si conduction band: $(x, -x, y, -y, z, -z)$. This defines the valley composition of each state. At the interface, the mass anisotropy breaks the valleys degeneracy in a doublet $(z, -z)$ and a quadruplet $(x, -x, y, -y)$. The doublet degeneracy is lifted due to the valley orbit coupling ($V_{\rm vo}^I = |V_{\rm vo}^I|e^{i\theta}$) arising in a sharp (001) interface,[9,12,14] as shown in (b). C_I^z and C_I^{-z} are defined in Eq. (6), and $\bar{C}_I^{-z} = -C_I^{-z}$. At an isolated donor, the valley orbit coupling leaves a non-degenerate ground state with A_1 symmetry, well separated (splitting ~ 12 meV) from the other five levels.[20–22] The binding energies given on the right of each level are experimental values for bulk P donors.[21] The lines join the valley compositions at donor and interface that are connected by symmetry.

barrier to Si, thus pushing the electron away from the donor and towards the interface (see Fig. 1(a)). In effective "atomic" units for Si, $Ry^* = m_\perp e^4/2\hbar^2\epsilon_{\rm Si}^2 = 19.98$ meV and $a^* = \hbar^2\epsilon_{\rm Si}/m_\perp e^2 = 3.157$ nm, the Hamiltonian is written as[8,19]

$$H = -\frac{\partial^2}{\partial x^2} - \frac{\partial^2}{\partial y^2} - \gamma\frac{\partial^2}{\partial z^2} - \frac{2}{r} + keFz + H_{\rm vo} \qquad (1)$$

with $\gamma = m_\perp/m_\parallel$ as the ratio between the transverse ($m_\perp = 0.191m$) and longitudinal ($m_\parallel = 0.916m$) effective masses, $\epsilon_{Si} = 11.4$, $k = 3.89 \cdot 10^{-7}\epsilon_{Si}^3(m/m_\perp)$cm/kV, and the electric field F is given in kV/cm. In Eq. (1), the kinetic energy is $(-\frac{\partial^2}{\partial x^2} - \frac{\partial^2}{\partial y^2} - \gamma\frac{\partial^2}{\partial z^2})$, the next two terms are the donor Coulomb potential and the electric-field linear potential, respectively. The last term describes the valley-orbit effects, namely the coupling between different valleys due to the singular nature of both the donor (D) and the interface (I) potentials, as described below.

As shown in Fig.1(a), the system can be modeled by

the combination of two potential wells: one that binds the electron to the donor (at low fields) and another binding the electron at the interface (at high fields).[8] Note that the interface potential includes not only the electric field perpendicular to the interface but also the Coulomb attraction to the donor at a distance d which confines the electron in the xy-plane even when it is at the interface.[7] We simplify the calculation by initially computing the variational ground state wave-functions at the donor and at the interface, which define the envelopes in the basis for the full six valley problem.

The conduction band of Si has six degenerate minima (valleys) in the $\langle 100\rangle$ directions at a distance $k_0 = 2\pi\frac{0.85}{a_{Si}}$ from the Γ point, where $a_{Si} = 5.4$Å is the lattice parameter of Si. In the simplest effective mass approximation, only the Bloch functions at the positions of the conduction band minima are considered, and the ground state of the electron at the donor is written[20]

$$\Psi_D = \sum_{\mu=\pm x,\pm y,\pm z} C_D^\mu F_D^\mu(\mathbf{r})\phi_\mu(\mathbf{r})\,, \tag{2}$$

where $F_D^\mu(\mathbf{r}) = F_D^{-\mu}(\mathbf{r})$ are envelope functions and $\phi_\mu(\mathbf{r}) = u_\mu(\mathbf{r})e^{i\mathbf{k}_\mu\cdot\mathbf{r}}$ are the six Bloch eigenstates at the conduction band minima. We take the variational donor envelope functions $F_D^\nu(\mathbf{r})$, where $\nu = |\mu|$, centered at $r = 0$, following the form introduced in Ref. [20]

$$F_D^x = N_D^x\, e^{-\sqrt{\frac{y^2+z^2}{a^2}+\frac{x^2}{b^2}}}\,, \tag{3}$$

$$F_D^y = N_D^y\, e^{-\sqrt{\frac{x^2+z^2}{a^2}+\frac{y^2}{b^2}}}\,, \tag{4}$$

$$F_D^z = N_D^z\, e^{-\sqrt{\frac{x^2+y^2}{a^2}+\frac{z^2}{b^2}}}\,. \tag{5}$$

These are normalized hydrogenic 1s envelopes, distorted due to the Si conduction band effective mass anisotropy, and $\{N_D^\nu\}$ are normalization factors. The effective Bohr radii a and b are variational parameters chosen to minimize the ground state energy. For the distances used here ($d \gtrsim 2a^* \approx 6$ nm), a and b coincide with Khon and Luttinger's variational parameters for a single impurity in the bulk[20] ($d \to \infty$), namely, $a = 2.365$ nm and $b = 1.36$ nm.[7]

The six-fold degeneracy of the ground state is lifted at a substitutional impurity because the translational symmetry of the host crystal is broken, leading to intervalley scattering effects known as the valley-orbit interaction.[23,24] This effect can be accounted for phenomenologically, introducing a coupling between valleys in perpendicular directions (e.g. x, z) $-\Delta_c$ and in parallel directions (e.g. $z, -z$) $-\Delta_c(1+\delta_c)$.[25] This splits the unperturbed six-fold-degenerate donor electron ground state into a singlet (A_1 symmetry), a triplet (T_2 symmetry) and a doublet (E symmetry), see Fig. 1. For P in Si, the relative splittings between the different symmetry levels are reproduced taking $\Delta_c = 2.16$ meV and $\delta = -0.3$.[25]

The degeneracy is also lifted near the (001) interface.[26,27] First, due to the mass anisotropy, the z and $-z$ perpendicular valleys are lower in energy than the ones parallel to the interface. The two lowest energy states are combinations of the z and $-z$ valleys, whose double degeneracy is lifted due to valley-orbit coupling $V_{\rm vo}^I$ at an abrupt interface. In general, $V_{\rm vo}^I$ is a complex quantity with an absolute value proportional to the applied electric field[9,12] $|V_{\rm vo}^I| = \lambda F$, and dependent on the barrier height and abruptness.[12] The prefactor λ has been estimated by several authors.[14] We use initially the largest, $\lambda = 1.36$ Å, as suggested in Ref. [11]. For instance, for $F = 50$ kV/cm, we have $|V_{\rm vo}^I| = 0.68$ meV. We also consider the smaller value of $\lambda = 0.215$Å, estimated by Sham and Nakayama,[9] and discuss the qualitative changes that occur in the spectrum. The complex phase of this valley-orbit coupling is also dependent on the interface quality and has been estimated to be ~ -1 for an abrupt Si/SiO_2 interface.[28] $H_{\rm vo}$ in Eq. (1) takes into account all these valley-orbit interactions, both at the donor (D) and at the interface (I). Its form (in a basis set defined next) is described in the Appendix.

Following Eq. (2), we take the lowest states at the interface as

$$\Psi_I = \sum_{\mu=\pm x,\pm y,\pm z} C_I^\mu F_I^\mu(\mathbf{r})\phi_\mu(\mathbf{r})\,. \tag{6}$$

The envelope functions $F_I^\nu(\mathbf{r})$, with $\nu = |\mu|$, are taken in the variational form[7]

$$F_I^x = N_I^x(z+d)^2 e^{-\alpha_{xy}(z+d)/2}e^{-(\beta_1 x^2+\beta_2 y^2)/2}\,, \tag{7}$$

$$F_I^y = N_I^y(z+d)^2 e^{-\alpha_{xy}(z+d)/2}e^{-(\beta_2 x^2+\beta_1 y^2)/2}\,, \tag{8}$$

$$F_I^z = N_I^z(z+d)^2 e^{-\alpha(z+d)/2}e^{-\beta^2\rho^2/2}\,, \tag{9}$$

where the penetration into the barrier is considered to be negligibly small. Here, $\rho^2 = x^2 + y^2$, and α, α_{xy}, β, β_1 and β_2 are variational parameters: $1/\alpha$ and $1/\alpha_{xy}$ are related to the width of the wave functions along the z-direction, and depend on the value of the applied electric field; β, β_1 and β_2 correspond to the confinement in the xy plane, which is controlled by the attractive potential of the donor, hence the "β" parameters depend on the distance d.[7]

In Eqs. (2) and (6) we do not include explicitly the pinning point for the plane-wave part of the Bloch functions at the the donor and interface potentials. Effects of the interference induced by the different pinning points are discussed in Ref. [18]. We solve for the lowest states of the full potential (donor, electric field and interface) by obtaining the spectrum of H in the combined basis of the lowest D and I envelopes as determined variationally, each multiplied by the respective Bloch functions. This defines the Hilbert space for our model calculation. States with different Bloch indices $\mu \neq \nu$ are not coupled unless there is a non-zero contribution from $H_{\rm vo}$ (see Appendix A). Within the Hilbert space defined here, the Hamiltonian is represented by a 12×12 matrix, written formally as four 6×6 blocks

$$H = \begin{bmatrix} H_{DD} & H_{ID} \\ H_{DI} & H_{II} \end{bmatrix} \tag{10}$$

The equation giving the spectrum takes into account the non-orthogonality of our basis, *i.e.*, we solve for $H\Psi_i = E_i S\Psi_i$, where S is the 12×12 overlap matrix so that $S^{\mu,\nu}_{DD} = S^{\mu,\nu}_{II} = \delta_{\mu\nu}$ and $S^{\mu,\nu}_{DI} = S^{\mu,\nu}_{ID} = \delta_{\mu\nu}\langle F^\mu_D \mid F^\mu_I\rangle$. Here, $\langle F^\mu_D \mid F^\mu_I\rangle$ is the overlap between the interface and the donor envelope functions, an exponentially decreasing function of d. A general state is written as:

$$\Psi = \sum_{\mu=\pm x,\pm y,\pm z} \sum_{L=I,D} C^\mu_L F^\mu_L(\mathbf{r})\phi_\mu(\mathbf{r})\,. \qquad (11)$$

The complex coefficients $\{C^\mu_L\}$ give the contributions to the state Ψ of each valley μ at the interface or donor ($L = I, D$). Also, they define the symmetry of the state, and are referred to here as "valley coefficients". The normalization condition reads

$$\sum_{\mu,\nu,L,L'} C^{\mu *}_L S^{\mu,\nu}_{LL'} C^\nu_{L'} = \sum_L |C^\mu_L|^2 + \text{cross terms} = 1, \qquad (12)$$

where the cross terms are zero for $L = L'$ and/or for $\mu \neq \nu$. For $d = 4a^*$ the cross terms due to the finite overlap between donor and interface envelopes are less than 5% in the electric field range of interest. The overlap S_{ID} is negligible for $d = 5a^*$ and larger.

In Fig. 1, we show the valley coefficients of the states at an isolated donor (just the $\{C^\mu_D\}$ are given since $C^\mu_I = 0$ for all μ) and at an interface under a perpendicular electric field (just the $\{C^\mu_I\}$ are given since $C^\mu_D = 0$ for all μ). The valley coefficients are perturbed when the impurity is located at a distance d from the interface, and hybrid states may be formed,[8,29] where both D and I coefficients contribute. The different initial (for low F) and final (for strong enough F) states are symmetry-compatible when their valley compositions are not orthogonal [see Fig.1 (main panel)].

III. RESULTS

Previous theoretical and experimental studies[8,17,29,30] identified and analyzed a characteristic field at which the electron ground state crosses over from being bound mainly around the donor (donor-like) into being bound mostly near the interface (interface-like). This field, $F_{\rm ch}$ (see Fig. 2), decreases with the distance d from donor to interface, while the tunneling time increases exponentially with d. These properties are consistent with our 6-valley model results. We explore here the valley degrees of freedom, mainly close to the characteristic field, and analyze how the applied field changes the valley composition of the main electronic states involved in the donor-interface shuttling.

The electric-field dependence of the complete spectrum of the Hamiltonian in Eq. (10), for $d = 4a^*$, is shown in Fig. 2. The overall level structure here is similar to the one presented in Refs. [15,17]. At small fields, $F \lesssim 32$ kV/cm, the six lowest eigenstates correspond to donor-bound states. The degeneracies of the T_2 triplet and

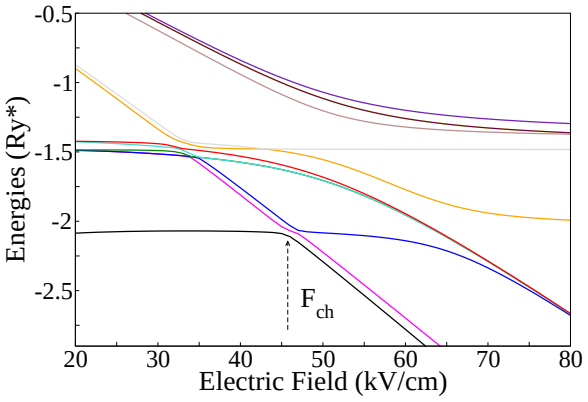

FIG. 2: (Color online) Full spectrum of eigenvalues for $d = 4a^*$ in a wide range of electric fields. For small values of the electric field, the lowest six eigenvalues correspond to the donor states and the highest six to interface states. We use here $V^I_{\rm vo} = |V^I_{\rm vo}|e^{i\pi/3}$ with $|V^I_{\rm vo}| = \lambda F$ and $\lambda = 1.36$ Å.

the E doublet are lifted (with a very small splitting) due to the perturbation produced by the interface. At large fields $F \gtrsim 70$ kV/cm, the six lowest eigenstates become interface-bound states. The two lowest eigenstates, which are combinations of the z and $-z$ valleys, are split by $2|V^I_{\rm vo}|$. Different eigenvalues cross over each other as F changes. The levels cross or anticross depending on their relative symmetry. The general scheme shown in Fig. 2 is qualitatively similar for different values of the distance d. The size of the gap at the anti-crossings is related to the shuttling time and decreases as d increases.[8]

We follow now on the evolution of the valley contributions of the three lowest eigenstates, which, via mutual energies crossing over, "become" or contribute to the ground state for some range of field values (see Fig. 3). Because of time-reversal symmetry, valleys μ and $-\mu$ contribute equally to any given eigenstate, so we may quantify the valley contributions by valley populations of each direction $\nu = x,\ y,\ z$, defined as

$$P_\nu = \sum_{\mu=\pm\nu} \sum_{L=I,D} |C^\mu_L|^2\,. \qquad (13)$$

Due to the cylindrical symmetry of the system, P_z is in general different from P_x and P_y, while the two latter are equivalent. This means that states with exchanged coefficients $C^{\pm x}_{L=I,D} \leftrightarrow C^{\pm y}_{L=I,D}$ give the same expectation value for the energy, since H is invariant under $\pm x \leftrightarrow \pm y$. So P_x and P_y are presumably equal. It may occur for a particular state that the weights P_x and P_y obtained numerically differ: in this case a degenerate state is always found with $P'_x = P_y$ and $P'_y = P_x$, as expected. Therefore, differences in P_x and P_y are not physically meaningful and we present our results in terms of P_z and

$$P_{xy} = (P_x + P_y)/2 = \frac{1}{2} \sum_{\mu=\pm x,\pm y} \sum_{L=I,D} |C^\mu_L|^2\,. \qquad (14)$$

In this definition we do not take the cross terms from Eq. (12) into account, so normalization gives $2P_{xy}+P_z \approx 1$, allowing P_z and P_{xy} to be directly compared to each other, giving the relative weight of the z and the average x and y populations. The lowest interface state at large F only involves z and $-z$ valleys, therefore $P_{xy} = 0$ and $P_z = 1$. On the other hand, the lowest donor state involves a symmetric combination of all valleys leading to $P_{xy} = P_z$. Hybrid states correspond to intermediate values of P_{xy} and P_z: $0 < P_{xy} < 1/3$ and $1/3 < P_z < 1$.

In Fig. 3 (upper frames) the spectrum is presented for a reduced range of energy and fields around the characteristic field for (a) $d = 4a^*$ ($F_{\rm ch} \sim 46$ kV/cm) and (b) $d = 5a^*$ ($F_{\rm ch} \sim 35$ kV/cm). The three rows of frames below give the corresponding valley populations for the 2$^{\rm nd}$ excited, 1$^{\rm st}$ excited, and ground (GS) states, respectively. Here we take a complex $V^I_{\rm vo} = |V^I_{\rm vo}|e^{i\pi/3}$. From Fig. 3 one can clearly observe that the anti-crossing at $F_{\rm ch}$ in fact involves two anti-crossings: one between GS and 1$^{\rm st}$ excited, and another one between 1$^{\rm st}$ and 2$^{\rm nd}$ excited states. Well below $F_{\rm ch}$, the GS is donor-like with $P_{xy} = P_z$. Above the two anti-crossings the GS and 1$^{\rm st}$ excited are interface-like states, only involving the z and $-z$ valleys, thus $P_{xy} = 0$.

We note that the ground state and the 2^{nd} excited state swap their valley compositions for fields below and above the crossover region. In fact, comparison of different frames in Fig. 3 show that the low-field D-like composition in (g) "moves" to the high-field behavior in (c), while the low-field I-like composition in (c) is found in the high-field behavior in (g). Along the crossover region the compositions change smoothly or abruptly (according to d) among the limiting behaviors. The same applies to frames (d) and (h) at a more distant donor position from the interface. The intermediate state, shown in (e) and (f), preserves the compositions at low and high fields, while it is clear that this state hybridizes with both ground and 2^{nd} excited states along the crossover region. In summary, the net effect of the field on the three lowest eigenfunctions far from F_{ch} is to cross the ground and 2^{nd} excited states, while the intermediate 1^{st} excited state is not affected overall, although all three states mix at the crossover range. An extreme example of the 1^{st} excited state not being affected by the crossover is discussed below, in the context of Fig.5.

Comparison between (a) and (b) in Fig. 3 illustrates the well known effect of increasing d, already discussed in previous publications,[7,8] namely reducing anti-crossing gaps and sharpening transition lines. Between the two anti-crossings, the 1$^{\rm st}$ excited state is donor-like for $d = 5a^*$ in Fig. 3(f), however for $d = 4a^*$ in (e) the 1$^{\rm st}$ excited state is an interface-donor hybrid due to the larger donor-interface overlap. We note that all the gaps obtained for $d = 5a^*$ are extremely small compared to the relevant energy scales here, so for most practical purposes the behavior would be equivalent to level crossing.

The phase θ on $V^I_{\rm vo} = |V^I_{\rm vo}|e^{i\theta}$, not as extensively considered so far, is analyzed in Fig. 4 for $d = 4a^*$. The

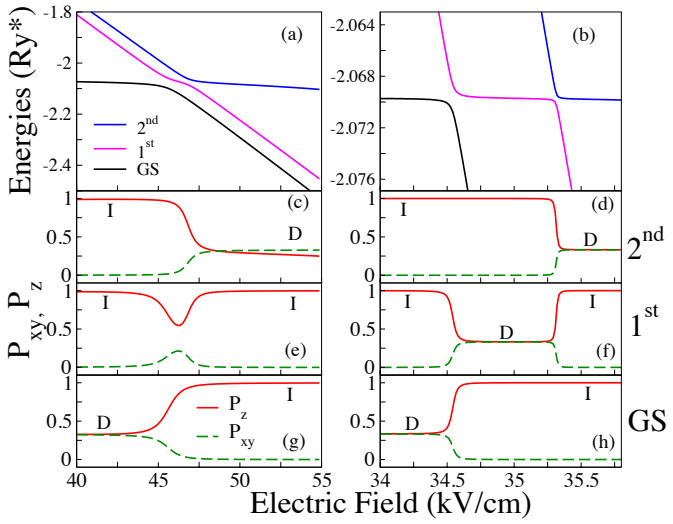

FIG. 3: (Color online) Evolution of the valley population for the three lowest eigenvalues around the characteristic field (see Fig. 2) for two different distances (a) $d = 4a^*$ and (b) $d = 5a^*$. We use $V^I_{\rm vo} = |V^I_{\rm vo}|e^{i\pi/3}$ with $|V^I_{\rm vo}| = \lambda F$ and $\lambda = 1.36$ Å. The top panels reproduce the eigenvalues involved in the lowest energy anti-crossing, which is in fact a sequence of two anti-crossings. All other panels show the valley population in the second excited state, the first excited state, and the ground state (GS) in different lines. The red (solid) curves correspond to the weight of the $\pm z$ valleys or longitudinal weight (at donor and interface), and the green (dashed) curves are the weight of the $\pm x$ and $\pm y$ valleys or transversal weight (at donor and interface). Labels D or I refer to donor-like or interface-like states in terms of real space location. Here D is a combination of the 6 valleys and I involves the z and -z valleys.

complex phase of the valley-orbit coupling at the interface affects the symmetries of the eigenstates leading to different gaps at the two anti-crossings around $F_{\rm ch}$. Figs. 4(a) and (g) show the limiting cases of $\theta = 0$ and $\theta = \pi$, which correspond to a real $V^I_{\rm vo}$, lead to a zero-gap (crossing) involving the symmetric donor-like eigenstate and the antisymmetric interface state, with all $C^\mu_L = 0$, except $C^z_I = -C^{-z}_I = 1/\sqrt{2}$. For a general θ, the two lowest interface states always have a symmetric component which "repel" the symmetric donor-like level. The size of the gap at the anti-crossing increases as the weight of the symmetric part of the interface-like state becomes larger. The two gaps become equal for $\theta = \pi/2$ which corresponds to a purely imaginary $V^I_{\rm vo}$. In summary, for a fixed $|V^I_{\rm vo}|$ and calling g_L and g_R the gaps to the left and to the right in energy, we get $g_L > g_R$ for $0 < \theta < \pi/2$ and $g_R > g_L$ for $\pi/2 < \theta < \pi$. In particular $g_R = 0$ ($g_L = 0$) for $\theta = 0$ (π) and $g_L = g_R$ for $\theta = \pi/2$. The largest gap observed for $d = 4a^*$ is ~ 1 meV, of the same order than the interface valley-orbit splitting considered. In contrast, for $d = 5a^*$ the gap is ~ 0.035 meV, almost two orders of magnitude smaller.

The results presented so far correspond to a relatively

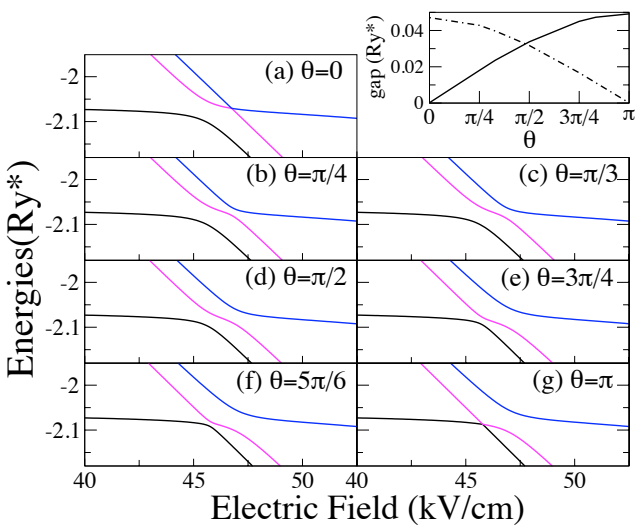

FIG. 4: (Color online) Three lowest eigenvalues around the anti-crossings region, corresponding to $d = 4a^*$ for different values of the phase θ of the valley-orbit coupling at the interface ($V_{\rm vo}^I = |V_{\rm vo}^I|e^{i\theta}$). $|V_{\rm vo}^I| = \lambda F$ and $\lambda = 1.36$ Å. The extra panel on the right top corner shows the values of the two anti-crossing gaps versus θ. The dashed line represents the gap for the first anti-crossing between the GS and the 1st excited state while the solid line is the gap between the 1st and 2nd excited states. Note that for $\theta = 0$ and π, $V_{\rm vo}^I$ is a real quantity and one of the anti-crossings has zero gap (namely, it is actually a 2-level crossing). The two gaps are equal for $\theta = \pi/2$ which corresponds to a pure imaginary $V_{\rm vo}^I$. Our results are obviously invariant for $\theta \leftrightarrow -\theta$.

large value of the valley-orbit coupling at the interface, with $\lambda = 1.36$ Å as estimated in Ref. [11]. For this case and $d = 4a^*$, the gap at anti-crossing is slightly smaller than the value of the valley-orbit splitting ($2|V_{\rm vo}^I|$). Previous calculations by Sham and Nakayama[9] lead to a smaller $\lambda = 0.215$Å. In Fig. 5 the three lowest eigenvalues close to the characteristic electric field for $d = 4a^*$ for the $V_{\rm vo}^I$ as calculated by Sham and Nakayama are shown. Here, the gap at anti-crossing (at $F = F_{\rm ch}$) is about three times larger than the value of the valley-orbit splitting at the interface for $d = 4a^*$. Due to the relatively smaller value of the valley-orbit splitting, the interface states are much closer: The two anti-crossings at $F_{\rm ch}$ seem to merge into a single one and the 1st excited state is always an interface state. This is in contrast with results for the larger value of $V_{\rm vo}^I$ where the 1st excited state is hybridized or donor-like between the two anti-crossings [see Fig.3(e) and (f)]. Another distinct feature of the small $|V_{\rm vo}^I|$ limit, illustrated in Fig. 5, [compare with Fig. 4(c)], is the way the three levels separate around $F_{\rm ch}$, with level repulsion among the outer ones, and no deviation of the middle state from the linear path: it does not couple to the others. Fig. 5 is very similar

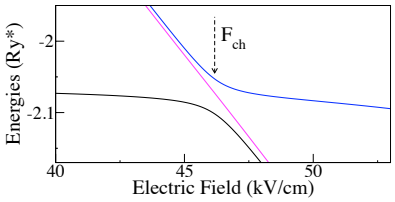

FIG. 5: (Color online) Three lowest eigenvalues for $d = 4a^*$ close to the characteristic field with the valley orbit coupling at the interface $|V_{\rm vo}^I| = \lambda F$ with $\lambda = 0.215$ Å as calculated by Sham and Nakayama.[9] We use $\theta = \pi/3$ as the phase of $V_{\rm vo}^I$ [compare with Fig. 4(c)].

to the inset of Fig. 2 in Ref. [15], where the model does not include a barrier, thus corresponding to the $V_{\rm vo}^I = 0$ limit. We may infer from these results that different ionization regimes for doped Si may arise as a function of d (inversely related to the gap at anticrossing) and the valley-orbit coupling at interface (related to the electric field, to the height, and to the quality of the interface barrier).

IV. DISCUSSION

We have analyzed in full depth the valley contributions to the three lowest energy levels of a single electron in the donor-in-Si-near-a-barrier system under an applied external field, focusing in the field range around the crossover between donor-like and interface-like character of the ground state. Strong hybridization occurs in the vicinity of the crossover, which we identify as a sequence of two anti-crossings (see Fig. 3). A result to keep in mind in practical applications is the strong dependence of the levels crossings and anti-crossings on the phase θ of the valley-orbit coupling at the interface, $V_{\rm vo}^I = |V_{\rm vo}^I|e^{i\theta}$. This is to be expected since the phases affect directly the symmetry of the states. A trivial example is the case $\theta = \pi$ (0), where the GS is a symmetric (anti-symmetric) combination of the z and $-z$ valleys. It is not a straightforward task to predict or control the phase θ, which should vary with the barrier material,[14] interface roughness due to steps, interdiffusion, etc, and other sample properties.

In practice, the results on the double anti-crossings shown in Fig. 4 may play an important role in applications involving the donor/barrier system. For instance, in the limit of $\theta \to 0$, the ground state is well separated from the excited states, suggesting the possibility of adiabatically shuttling the electron from the donor site to the barrier interface. This could be a suitable scenario for a spin qubit for which one needs the valley splitting to be larger than the Zeeman splitting. An intrinsically large $|V_{\rm vo}^I|$, like the one considered in Figs. 2, 3, and 4, is also needed, as well as a small d ($\lesssim 4a^*$) to guarantee a sufficiently large gap at anticrossing.

On the other hand, following the adiabatic theorem, the donor-interface shuttling would be prohibitively slow for $\theta \to \pi$ due to the crossing between the ground state and the first excited level. Another phase-related effect occurs due to the variable pinning point in the Bloch functions $\phi_\mu(\mathbf{r})$ [18,31], which produces a periodic dependence of the valley-orbit splitting on d leading to the closing of the gap at anticrossings at some particular values of d [18].

If instead of the spin we want to use the valley degree of freedom to define qubits, a controllable valley-orbit coupling is required.[5] This is achieved if the energy separation of two states with the same envelope function but different valley compositions (therefore, different oscillations in the atomic scale) varies significantly with the external applied fields. This situation can be attained above $F_{\rm ch}$ when the two lowest eigenstates are mainly interface states involving different combinations of the z and $-z$ valleys. A strong dependence of the splitting with electric field can be found close to $F_{\rm ch}$ in some cases. For instance, in Fig. 4(g) (corresponding to $\theta = \pi$) the closing of the gap between the two lowest eigenvalues produces a fast decrease of the splitting as the electric field is lowered from ~ 48 to ~ 46 kV/cm. Also, for smaller values of $V_{\rm vo}^I$, as exemplified in Fig. 5, the interface-donor hybridization leads to a relatively large gap compared to $V_{\rm vo}^I$ and consequently the splitting increases fast from ~ 48 to ~ 46 kV/cm. However, the variation of the level splitting on the electric field is stronger when the donor-interface hybridization is large. This hybridization mixes valleys in the different directions, potentially producing decoherence in the valley sector.

On the other extreme, $\theta = 0$, Fig. 4(a) reveals that the upper valley composition crosses the second excited state: As a consequence, the valley information would be lost.

In summary, we show that both the modulus and the phase of $V_{\rm vo}^I$ affect the quantum behavior of donor electrons in Si near an interface. The value of θ is hard to predict, and its calculation probably requires knowledge of the atomistic distribution at the interface and a complete electronic structure description of the combined Si/structured interface/barrier system. It is not clear whether a direct experimental measure is possible. We propose that measurement of the separate gaps may provide an estimate of θ, as shown in the inset of Fig. 4. Finally, the trends and discussions regarding Fig.3 should bring new and valuable insight towards controlled valley manipulations.

A.B. and M.J.C. were supported by FIS2009-08744 (MINECO, Spain). AS and BK's work is part of the Brazilian National Institute for Science and Technology on Quantum Information. AS and BK acknowledge partial support from FAPERJ, CNPq and CAPES

Appendix A: Valley-orbit term ($H_{\rm vo}$)

The last term in Eq. (1), with $\Delta_\perp = -\Delta_c = -2.16$ meV, $\Delta_\parallel = -\Delta_c(1+\delta_c) = -1.51$ meV, and $|V_{\rm vo}^I| = \lambda F$ with $\lambda = 1.36$ Å. This is a 12x12 matrix in the basis set of the six valleys at the donor and the six valleys at the interface. According to the notation in Eq. (10):

$$[H_{\rm vo}]_{DD} = \begin{pmatrix} 0 & \Delta_\parallel & \Delta_\perp & \Delta_\perp & \Delta_\perp & \Delta_\perp \\ \Delta_\parallel & 0 & \Delta_\perp & \Delta_\perp & \Delta_\perp & \Delta_\perp \\ \Delta_\perp & \Delta_\perp & 0 & \Delta_\parallel & \Delta_\perp & \Delta_\perp \\ \Delta_\perp & \Delta_\perp & \Delta_\parallel & 0 & \Delta_\perp & \Delta_\perp \\ \Delta_\perp & \Delta_\perp & \Delta_\perp & \Delta_\perp & 0 & \Delta_\parallel \\ \Delta_\perp & \Delta_\perp & \Delta_\perp & \Delta_\perp & \Delta_\parallel & 0 \end{pmatrix} \tag{A1}$$

$$[H_{\rm vo}]_{II} = \begin{pmatrix} 0 & 0 & 0 & 0 & 0 & 0 \\ 0 & 0 & 0 & 0 & 0 & 0 \\ 0 & 0 & 0 & 0 & 0 & 00 \\ 0 & 0 & 0 & 0 & 0 & |V_{\rm vo}^I|e^{i\theta} \\ 0 & 0 & 0 & 0 & |V_{\rm vo}^I|e^{-i\theta} & 0 \end{pmatrix} \tag{A2}$$

and $[H_{\rm vo}]_{ID} = [H_{\rm vo}]_{DI} = 0$.

[1] M. A. Nielsen and I. L. Chuang, *Quantum Computation and Quantum Information* Cambridge University Press, Cambridge (2000).

[2] B. E. Kane, Nature **393**, 133 (1998).

[3] S. Das Sarma, R. de Sousa, X. Hu, and B. Koiller, Solid State Communications**133**, 737 (2004).

[4] D. P. DiVincenzo, Science **270**, 255 (1995).

[5] D. Culcer, A. L. Saraiva, B. Koiller, X. Hu, and S. Das Sarma (2011), Phys. Rev. Lett. **108**, 126804 (2012)

[6] G. C. Tettamanzi, J. Verduijn, G. P. Lansbergen, M. Blaauboer, M. J. Calderón, R. Aguado and S. Rogge, Phys. Rev. Lett. **108**, 046803 (2012).

[7] M. J. Calderón, B. Koiller, and S. Das Sarma, Phys. Rev. B **75**, 125311 (2007).

[8] M. J. Calderón, B. Koiller, X. Hu, and S. Das Sarma, Phys. Rev. Lett. **96**, 096802 (2006).

[9] L. J. Sham and M. Nakayama, Phys. Rev. B **20**, 734 (1979).

[10] S. Goswami, K. A. Slinker, M. Friesen, L. M. McGuire, J. L. Truitt, C. Tahan, L. J. Klein, J. O. Chu, P. M. Mooney, D. W. van der Weide, et al. , Nat. Phys. **3**, 41 (2007).

[11] S. Chutia, S. Coppersmith, and M. Friesen, Phys. Rev. B **77**, 193311 (2008).

[12] A. L. Saraiva, M. J. Calderón, X. Hu, S. Das Sarma, and B. Koiller, Phys. Rev. B **80**, 081305 (2009).

[13] W. H. Lim, C. H. Yang, F. A. Zwanenburg, and A. S. Dzurak, Nanotechnology **22**, 335703 (2011).

[14] A. L. Saraiva, M. J. Calderón, R. B. Capaz, X. Hu, S. Das Sarma, and B. Koiller, Phys. Rev. B **84**, 155320 (2011).

[15] A. Debernardi, A. Baldereschi, and M. Fanciulli, Physical Review B **74**, 035202 (2006).

[16] A. Debernardi, A. Baldereschi, and M. Fanciulli, Physical Review B **81**, 195302 (2010).
[17] R. Rahman, G. P. Lansbergen, S. H. Park, J. Verduijn, G. Klimeck, S. Rogge, and L. C. L. Hollenberg, Phys. Rev. B **80**, 165314 (2009).
[18] M. J. Calderón, B. Koiller, and S. Das Sarma, Phys. Rev. B **77**, 155302 (2008).
[19] D. MacMillen and U. Landman, Phys. Rev. B **29**, 4524 (1984).
[20] W. Kohn and J. M. Luttinger, Phys. Rev. **98**, 915 (1955).
[21] T. Ning and C. Sah, Phys. Rev. B **4**, 3468 (1971).
[22] B. Koiller, X. Hu, and S. Das Sarma, Phys. Rev. Lett, **88**, 027903 (2001).
[23] A. Baldereschi, Phys. Rev. B **1**, 4673 (1970).
[24] S. T. Pantelides, Rev. Mod. Phys. **50**, 797 (1978).
[25] B. Koiller, X. Hu, and S. Das Sarma, Phys. Rev. B **66**, 115201 (2002).
[26] T. Ando, A. B. Fowler, and F. Stern, Rev. Mod. Phys. **54**, 437 (1982).
[27] B. E. Kane, Fortschr. Phys. **8**, 1023 (2000).
[28] Data taken from Fig. 2 in Ref. 14. Note that in that figure the labels for $\mathrm{Re}V^I_{\mathrm{vo}}$ and $\mathrm{Im}V^I_{\mathrm{vo}}$ are accidentally interchanged.
[29] A. S. Martins, R. B. Capaz, and B. Koiller, Phys. Rev. B **69**, 085320 (2004).
[30] G. P. Lansbergen, R. Rahman, C. J. Wellard, I. Woo, J. Caro, N. Collaert, S. Biesemans, G. Klimeck, L. C. L. Hollenberg, and S. Rogge, Nature Physics **4**, 656 (2008).
[31] B. Koiller, R. B. Capaz, X. Hu, and S. Das Sarma, Phys. Rev. B **70**, 115207 (2004).